Sources of errors in spatial frequency domain imaging of scattering media

Nico Bodenschatz
Arnd Brandes
André Liemert
Alwin Kienle

Sources of errors in spatial frequency domain imaging of scattering media

Nico Bodenschatz,* Arnd Brandes, André Liemert, and Alwin Kienle
Institut für Lasertechnologien in der Medizin und Meßtechnik, Helmholtzstr. 12, D-89081 Ulm, Germany

Abstract. Knowledge of the impact of potential sources of error in spatial frequency domain imaging (SFDI) is essential for the quantitative characterization of absorption and scattering in tissue and other turbid media. We theoretically investigate the error in the derived absorption and scattering parameter, subject to typical experimental and theoretical sources of errors. This provides a guideline to properly assess the significance of various parameters related to the measurement and the theoretical evaluation of spatial frequency domain reflectance data. At the same time, this study serves as a reference to estimate the overall precision of derived optical parameters of semi-infinite scattering media using SFDI. © *2014 Society of Photo-Optical Instrumentation Engineers (SPIE)* [DOI: 10.1117/1.JBO.19.7.071405]

1 Introduction

Spatial frequency domain imaging (SFDI) is a promising technique for the characterization of absorption and scattering in turbid media. Over the last decade, its principal capability to map optical properties in both phantoms and human or animal tissues has been successfully demonstrated.[1–9] The technique employs spatially modulated light-intensity projections and captures the diffuse reflectance signal with a digital camera. The obtained spatially resolved intensity can be used to inversely derive optical scattering and absorption parameters. These parameters carry useful information about the metabolic and structural tissue properties.[5–7,9] Tissue absorption is typically linked to metabolic properties like perfusion, oxygenation, and chemical content, whereas tissue scattering is more related to structural properties like cell density or tissue type. Therefore, it is crucial to understand the overall precision of derived scattering and absorption values in order to correctly interpret the tissue optical properties. We seek to enhance this understanding by our subsequent error analysis.

In the first part of our study (Sec. 2), we focus on errors connected to the theoretical evaluation of SFDI data. In this context, we investigate the significance of applying the correct scattering phase functions and analyze the impact of possible errors in refractive index. Furthermore, the common errors associated with the diffusion approximation to radiative transfer are examined.

In the second part (Sec. 3), we shift the focus to experimental sources of error such as incorrect height adjustment, projection boundary effects, binning errors, and errors in the assumed spatial frequency. Based on our comprehensive error analysis, we finally discuss the overall precision of derived optical parameters using SFDI.

SFDI is typically used to extract the reduced scattering coefficient μ_s' from the experimental data, as it is a much better indicator for the turbidity of a system than the scattering coefficient μ_s, which quantifies the frequency but not the efficiency of scattering. The derivation of $\mu_s' = \mu_s(1 - g)$ is, however, still slightly dependent on the assumption for the asymmetry parameter $g = \langle \cos(\theta) \rangle$, which is the mean cosine of the scattering angle θ for a single scattering event. This dependency will be analyzed in Sec. 2.1.

The sensitivity of SFDI varies with the reduced scattering μ_s' and absorption μ_a. Likewise, most errors in SFDI are dependent on the scattering and absorption regime. Therefore, our error analysis takes into account this dependency on μ_a and μ_s' and considers the absorption regime $0.003 \text{ mm}^{-1} \leq \mu_a \leq 0.3 \text{ mm}^{-1}$ and assumes the reduced scattering to be in the range of $0.5 \text{ mm}^{-1} \leq \mu_s' \leq 5 \text{ mm}^{-1}$. These absorption and scattering ranges contain all optical properties typically found for biological tissue.[10]

In order to best comprehend the impact of various sources of error, we assume semi-infinite and both homogeneously and isotropically scattering media with the vertical projection of spatially modulated sinusoidal patterns. Unless stated otherwise, the surface of the media is assumed to be ideally flat and the real part of the refractive index is set to $n_r = 1.4$ and $n_r = 1.0$ inside and outside the media, respectively. Specular reflection of the incident light pattern is disregarded for all subsequent analysis.

For the most part of our study, we model spatial frequency reflectance using the Henyey–Greenstein scattering phase function with asymmetry $g = 0.9$, which is a typical value found for biological tissue.[10,11] Both experimentally and especially on a theoretical level, the use of only two spatial frequencies is sufficient for accurate derivation of both optical parameters. Relating to the average of many experimental studies,[2–5,12] we make use of two spatial frequencies, namely $f = 0 \text{ mm}^{-1}$ and $f = 0.24 \text{ mm}^{-1}$ ($k = 0 \text{ rad mm}^{-1}$ and $k = 1.5 \text{ rad mm}^{-1}$). The use of more intermediate frequencies may be experimentally advantageous, but generally does not provide additional

*Address all correspondence to: Nico Bodenschatz, E-mail: nico.bodenschatz@ilm.uni-ulm.de

information for semi-infinite and homogeneously scattering media. Nevertheless, some of the presented errors also depend on the spatial frequency range and this dependency will be discussed in the corresponding sections.

2 Analysis of Errors Related to Theoretical Assumptions

In this section, theoretical assumptions that typically arise in the evaluation process of spatial frequency domain (SFD) reflectance data are examined. The term SFD reflectance always denotes the amplitude of the diffuse reflectance signal and in the following, we consider three sources of errors and their impact on the derived absorption and scattering coefficients. In a first step, the relevance of the scattering phase function and its scattering asymmetry $g = \langle \cos(\theta) \rangle$ on the derived parameters μ_a and μ_s' is studied. Afterward, further analysis is done on the error which corresponds to the diffusion approximation and which reduces the scattering phase function to its simplest form. Finally, errors in the refractive index are characterized as one further source of error in SFDI.

The presented sources of error may have similar relevance for other diffuse optical imaging techniques. As will be shown, the impact of some of the presented errors varies strongly with the spatial frequency. Errors that manifest themselves at high spatial frequencies in SFDI will have similar relevance in real domain spatially resolved systems, when looking at proximal detection of photons. Nevertheless, focus of all subsequent analysis is the qualitative dependency of errors over the SFD together with a quantitative error analysis for a typical pair of spatial frequencies.

2.1 Scattering Phase Function

Derivation of optical scattering and absorption parameters in SFDI is usually either performed by look-up-table methods in connection with Monte Carlo simulations[7,9] or by relying on the diffusion approximation to radiative transfer.[2–5] Recently, an analytical solution to the radiative transfer equation for semi-infinite media has been found.[13,14] This solution allows for both fast and accurate modeling and evaluation of SFD reflectance data. Both the use of Monte Carlo simulations and analytical solutions to radiative transfer requires adequate choice of the scattering phase function $p(\theta)$. This function is often unknown or approximated by analytical expressions which are easy to work with, such as the Henyey–Greenstein function.[15] Due to its mathematical simplicity, this is one of the most widely applied scattering phase functions in diffuse optical imaging and beyond.[9,15] Therefore, we start by modeling SFD reflectance using the Henyey–Greenstein function and compare it to that of three different functions with identical asymmetry $\langle \cos(\theta) \rangle$. Afterward, we only focus on the Henyey–Greenstein phase function and investigate the effect of its asymmetry parameter, which can be easily adapted to approximate the light scattering in various media. In this context, the significance of a change in g on the derived optical parameters is presented.

The inset of Fig. 1 depicts four different scattering phase functions on a semi-log-scale with equal asymmetry $g = 0.9$. In particular, the Henyey–Greenstein function is compared to Mie scattering and two Reynolds–McCormick (Gegenbauer kernel) scattering functions.[16] Note that the Henyey–Greenstein function equates to a Reynolds–McCormick function with its second input parameter set to $\alpha = 0.5$. We therefore choose
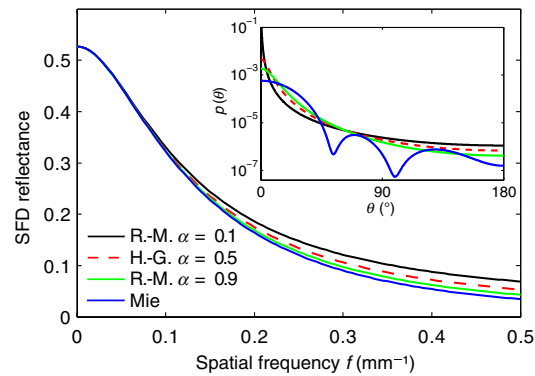

Fig. 1 Modeled spatial frequency domain (SFD) reflectance versus spatial frequency f at $\mu_s' = 1.6$ mm^{-1} and $\mu_a = 0.03$ mm^{-1} for four different scattering phase functions $p(\theta)$. The corresponding phase functions share the asymmetry $g = 0.9$ and are depicted in the inset.

$\alpha = 0.9$ and $\alpha = 0.1$ for the two other Reynolds–McCormick functions for modeling of more or less pronounced forward scattering, respectively. The selected Mie phase function corresponds to a sphere of 0.5 μm diameter with a refractive index mismatch of $\Delta n_r = 0.1$ between its inside and outside, which is illuminated by a plane wave with a wavelength of $\lambda = 650$ nm in the surrounding medium.

The main graph in Fig. 1 exemplifies SFD reflectance for all four phase functions versus spatial frequency for $\mu_a = 0.03$ mm^{-1} and $\mu_s' = 1.6$ mm^{-1}. These curves are derived from Monte Carlo simulations using point illumination of a semi-infinite media with spatially resolved detection of photons at the medium boundary. A convolution of this spatially resolved reflectance with different spatial frequency patterns (i.e., sine waves) is then used to derive the SFD reflectance signal. Noticeably, the four curves almost coincide for $f = 0$ mm^{-1} and their deviation increases with spatial frequency. This deviation is more pronounced in the low scattering regime and almost independent of absorption (assuming 0.003 mm$^{-1} \leq \mu_a \leq 0.3$ mm^{-1}). The deviation in SFD reflectance for differing phase functions at high spatial frequencies can be understood from the corresponding strong sensitivity to short-range photons (i.e., light reflected in proximity to its entry point). Sampling of these photons is enhanced for more intense scattering at larger scattering angles, as observed for the Reynolds–McCormick phase function with $\alpha = 0.1$.

In the following, SFD reflectance data are computed for various combinations of μ_a and μ_s', similar to the reflectance curves in Fig. 1. Afterward, data corresponding to Reynolds–McCormick ($\alpha = 0.1$ and $\alpha = 0.9$) or Mie scattering are evaluated at two spatial frequencies ($f = 0$ mm^{-1} and $f = 0.24$ mm^{-1}) incorrectly assuming Henyey–Greenstein scattering. This and all subsequent fitting procedures are performed using the Gauss–Newton algorithm. Thereby, one arrives at optical parameters which deviate from their original values. This deviation $\Delta \mu_s'$ and $\Delta \mu_a$ is strongly dependent on the scattering regime and almost independent of absorption. Figure 2 gives the obtained relative error of μ_s' over a wide scattering range for the three different phase functions.

The relative error of μ_a is almost identical to that of μ_s' and therefore not shown in a separate graph. This similarity in both errors can be qualitatively understood from a scaling property in SFDI. We can observe in Fig. 1 that the variation of the scattering function is very similar to spatial frequency scaling when
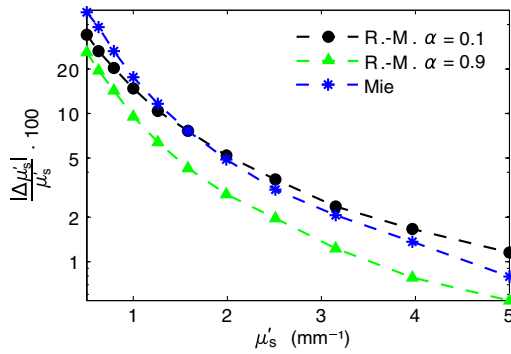
Fig. 2 Relative error of μ_s' in percent due to an incorrect scattering phase function. Here, we use the Henyey–Greenstein function to evaluate SFD data which corresponds to Reynolds–McCormick or Mie scattering. The obtained relative error in μ_a (not shown) is almost identical to that of μ_s'.

Fig. 3 Relative error in μ_s' in percent related to an incorrect assumption of the asymmetry value g. SFD data were calculated for four reduced scattering values with $g = 0.9$ and evaluated assuming different g-values. The obtained error scales almost linearly with the incorrectness in g. The corresponding relative error in μ_a (not shown) is almost identical to that of μ_s'.

considering the effect on SFD reflectance. As will be discussed in Sec. 3.4, spatial frequency scaling relates to the scaling of μ_a and μ_s' by a common factor and can therefore account for the similarity in both errors.

As can be seen in Fig. 2, large errors arise from the choice of incorrect scattering phase functions in both scattering and absorption. These errors are profound in the low scattering regime, where high spatial frequencies relate to photons, which have undergone only a few scattering events.[17] Therefore, one should carefully consider the phase function of less intensely scattering media. As a consequence, comparative studies across different absorption or scattering regimes (such as dilution series) or spectrally resolved measurements to compute absorption spectra may be falsified by the unawareness of the correct scattering phase function. Note, however, that in order to separate this analysis from our successive study on the scattering asymmetry, we chose all four functions such that $g = 0.9$.

In the next step, the influence of the scattering asymmetry g is studied. We do this by calculation of SFD reflectance data for $g = 0.9$ using the analytical radiative transfer solution[13] and the Henyey–Greenstein function. Subsequently, these data are evaluated by means of the same analytical solution assuming incorrect values of g. In consequence, incorrect values for μ_s' and μ_a are obtained. Figure 3 gives the relative error of μ_s' as a function of the assumed asymmetry value g for four different scattering regimes.

Variation in scattering asymmetry changes SFD reflectance in a way similar to variations in the scattering phase function (see Fig. 1). Likewise, SFD reflectance is mostly affected at higher spatial frequencies and the relative error in μ_a related to the asymmetry parameter is almost equal to that of μ_s' (see Fig. 3) and therefore not shown.

According to Fig. 3, no error in μ_s' is obtained for $g = 0.9$ as this asymmetry agrees with the previously calculated reflectance data. The more the assumption for g deviates from the actual asymmetry value, the higher the obtained relative error in μ_s'. The deviation of the four data curves shows larger errors for media with low scattering. This is because a reduction in μ_s' (and μ_a) corresponds to an upscaling in spatial frequency and thus to a larger deviation in SFD reflectance, as will be further discussed in Sec. 3.4. At the same time, the relative error in μ_s' is almost independent of the absorption regime. This is indicated by the error bars of the data points in Fig. 3, which correspond to
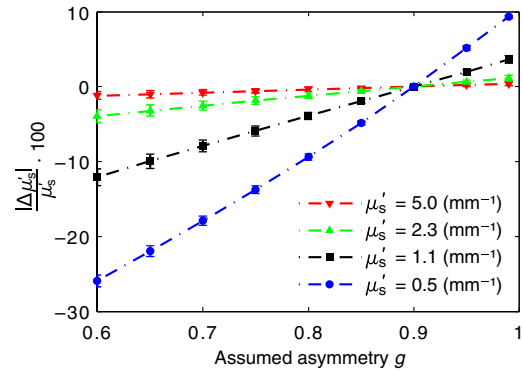
the standard deviation for analogous computations over a wide absorption regime ($0.003 \text{ mm}^{-1} \leq \mu_a \leq 0.3 \text{ mm}^{-1}$).

2.2 Diffusion Approximation

Having studied the potential error related to the scattering phase functions, we now concentrate on the evaluation theories for SFDI in general. Particularly, we are interested in the error related to the diffusion approximation to radiative transfer, where the angular scattering characteristics of single scatterers are almost completely neglected.

Data evaluation in SFDI is frequently approximated by diffusion theory due to its simplicity and very high computational speed. In contrast, Monte Carlo simulations can be more accurate, but suffer from relatively long yet decreasing[18] computational times. In order to study the frequently accepted error[2–5] associated with the diffusion approximation, we use our analytical solution to the radiative transfer equation[13,14] for the computation of SFD reflectance data at the frequencies $f = 0 \text{ mm}^{-1}$ and $f = 0.24 \text{ mm}^{-1}$. Thereby, we assume the Henyey–Greenstein function with $g = 0$. This computation is performed systematically for various absorption and scattering combinations and the obtained reflectance data are evaluated using the corresponding diffusion approximation for the same experimental geometry[12] and a nonlinear regression routine. Thereby, one arrives at scattering and absorption values, which deviate from the correct optical parameters. This deviation is shown in two contour plots in Figs. 4 and 5, where different contour levels correspond to different relative errors in μ_a and μ_s', respectively.

We observe that the diffusion approximation causes errors which largely depend on the absorption and scattering regime. Expectedly, largest errors are found for media of low scattering and high absorption, where the preconditions for the diffusion approximation are least fulfilled. However, even with highly scattering media, errors in excess of 10% can arise. For high scattering, we learn from Figs. 4 and 5 that diffusion theory underestimates both μ_a and μ_s'. This can be understood from the corresponding overestimation of short-range photons in diffusion theory.

Based on this error analysis, the benefit of an analytical radiative transfer model for SFDI can be quantitatively understood.
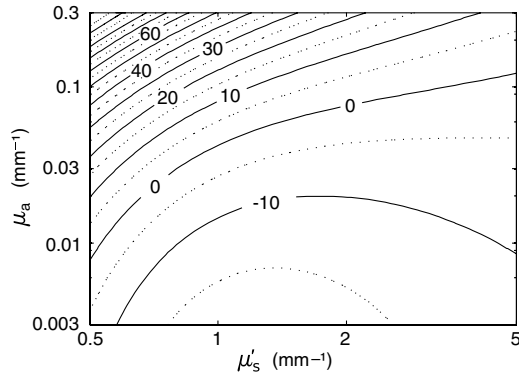
Fig. 4 Relative error of the absorption coefficient $\Delta\mu_a/\mu_a$ in percent due to the diffusion approximation. The contour lines give the error over a wide scattering and absorption regime.

Similarly, also combined Monte Carlo look-up-table approaches have the potential to overcome the presented errors, which may be large for particular combinations of μ_a and μ_s' even in the very high scattering and low absorption regime.

2.3 Refractive Index

The refractive indices of most samples investigated in SFDI are oftentimes only approximately known. Typically, the real part of the refractive index of biological tissue is in the range of $1.35 \leq n_r \leq 1.50$ with some wavelength dependency of about 1% across the optical window (650 nm $\leq \lambda \leq$ 1050 nm).[19–21] Uncertainty in refractive index implies inaccuracy in the derived optical parameters. In the following section, this inaccuracy in determining μ_a and μ_s' is quantified as a function of the error in refractive index Δn_r. It should be noted that we consider the average refractive index of the scattering media and not that of single scattering particles. In consequence, we still make the simplifying assumption of a homogeneously scattering media with scattering and absorption properties, that are independent of the media's refractive index. Therefore, the assumed refractive index value merely controls the amount of transmitted and reflected light on both sides of the medium surface, as given by the Fresnel equations. In order to study the impact of the refractive index on the derived absorption and scattering coefficients, we calculate SFD reflectance using our analytical
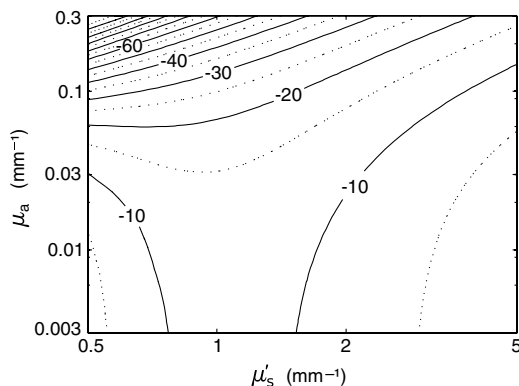

Fig. 6 Relative error of the absorption coefficient $\Delta\mu_a/\mu_a$ in percent for incorrect assumption of the refractive index. Here, the refractive index is assumed to be too large by $\Delta n_r = 0.05$. SFD reflectance data were calculated for $n_r = 1.4$ and evaluated assuming $n_{r,err} = n_r + \Delta n_r = 1.45$.

radiative transfer solution for semi-infinite media assuming a refractive index of $n_r = 1.40$. Subsequently, this data is evaluated by falsely assuming $n_{r,err} = 1.45$ which ultimately produces errors in μ_a and μ_s'. Figures 6 and 7 give these relative errors in absorption and scattering, respectively, over a wide scattering and absorption range.

An increase in the refractive index increases both the amount of specularly reflected light at the medium surface and the number of diffuse photons reflected at the internal medium boundary. In our analysis, we focus only on the latter effect, since specular reflections have a strong dependence on surface properties of the sample and are oftentimes avoided by oblique projection[2–7,9,12,22] and the use of crossed-linear polarizers.[2–6,9,22] The effect of the internal reflection increases the average lateral propagation distance of diffuse light inside the media. This increases the probability for absorption and reduces SFD reflectance especially for high spatial frequencies. Hence, an overestimation in the refractive index is mostly compensated by an apparent decrease in absorption or an apparent increase in scattering.

Qualitatively, the two contour plots in Figs. 6 and 7 are also correct for different errors Δn_r. Our computations show that the relative error in μ_a and μ_s' is almost linearly proportional to Δn_r in the range $1.35 \leq n_r \leq 1.50$. It is therefore possible to simply

Fig. 5 Relative error in the reduced scattering coefficient $\Delta\mu_s'/\mu_s'$ due to the diffusion approximation. The contour lines give the relative error in percent and as a function of the scattering and absorption coefficients.
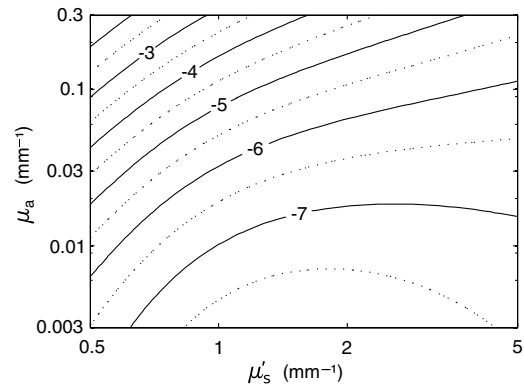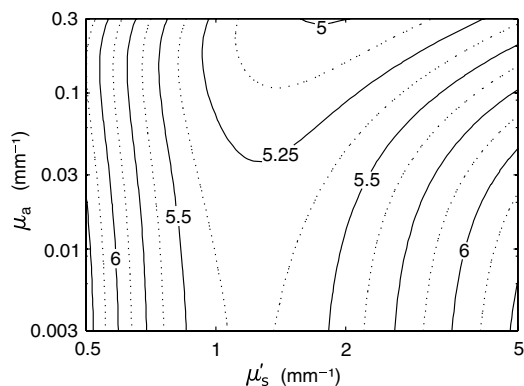

Fig. 7 Relative error in the reduced scattering $\Delta\mu_s'/\mu_s'$ in percent over a wide absorption and scattering range for an error in refractive index of $\Delta n_r = 0.05$.

scale the contours in Figs. 6 and 7 by $\Delta n_r/0.05$ to obtain the error for any uncertainty Δn_r in the refractive index.

3 Analysis of Errors Related to the Experimental Parameters

In the following sections, we focus on sources of error which are more related to the collection of experimental data in the SFD. In particular, we study four experimental sources of error, namely projection boundary effects, binning of SFD images, inaccuracies in the sample-camera distance, and errors due to improper calibration of spatial frequencies.

3.1 Projection Boundary Errors

Experimentally, the projection of spatial frequency patterns is typically restricted to a limited spatial projection area. This gives rise to boundary effects close to the border of the projection field. Underneath projection boundaries, diffusing light scatters away from the projection area without being compensated by diffuse light from outside the projection field. Therefore, reflectance at $f = 0$ mm^{-1} [which is typically denoted as direct current (DC) component] decreases and approaches zero at further distance from the projection area.

A similar effect is observed for experiments on phantoms, where the finite phantom size causes a drop in reflectance near the phantom boundaries. This decline is even larger than that of the projection boundaries, since diffusing light which leaves the phantom to the side cannot scatter back into the media.

The SFD reflectance for frequencies above zero is usually termed AC component and is calculated using the following formula:

$$\mathrm{AC} = \frac{\sqrt{2}}{3}\sqrt{(R_0 - R_{2\pi/3})^2 + (R_{2\pi/3} - R_{4\pi/3})^2 + (R_{4\pi/3} - R_0)^2},$$
(1)

where R_0, $R_{2\pi/3}$, and $R_{4\pi/3}$ are the three phase projections with zero, 120 and 240 deg phase shift.[2,4,6,12] However, due to overall decline in reflectance across the projection boundaries for all three phase projections, the AC component as computed with Eq. (1) undergoes strong oscillations and is no longer properly determined. At the same time, the DC component, which is the average reflectance of the three phase projections, decreases smoothly at the projection boundaries.

We are interested in an estimation of the required distance from the projection boundaries for the error in SFD reflectance to be below 1% for both spatial frequencies (DC and AC components). Figure 8 gives this distance in millimeters by means of a contour plot as a function of reduced scattering and absorption. The data are based on Monte Carlo simulations for semi-infinite media with vertical point illumination and spatially resolved detection of photons at the medium boundary. A convolution of this reflectance signal with a finite sinusoidal projection pattern is used to compute the change in SFD reflectance at the projection boundaries. Upon the examination of Fig. 8, it is important to understand that an error of 1% in reflectance may give rise to a relative error in μ_a or μ_s' of several percents. Due to strong oscillation of the AC component at the projection boundaries, as calculated by Eq. (1), it is however difficult to directly state the errors in μ_a and μ_s', as they depend on the relative behavior of the DC and the AC components. As a rule of thumb, the relative error in μ_a and μ_s' for the stated distances
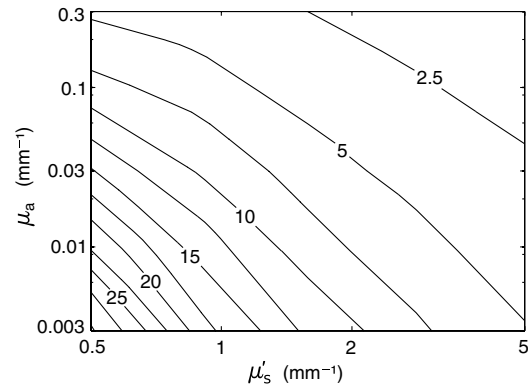

Fig. 8 Required distance from the projection boundaries in millimeters in order to achieve a deviation in SFD reflectance of <1%. Doubling of the stated values gives an error in SFD reflectance of <0.1%.

from the projection boundaries (see Fig. 8) is mostly within 5%. Our computations show that the absorption parameter is more sensitive to small deviations in reflectance than the reduced scattering parameter μ_s'. Indeed, the obtained error in μ_s' is often below 2% for errors in reflectance below 1%. However, in the very low absorption and high scattering regime, the error in μ_a may rise to values close to 20% for the same accuracy in reflectance. Especially in this regime, the experimentalist is advised not to consider SFD data closer than twice the values stated in Fig. 8, thus achieving an error of < 0.1% in (both DC and AC) reflectance.

Accuracy in SFD reflectance close to the projection boundaries is to a smaller extent also dependent on the spatial frequency. The presented boundary errors are based on the spatial frequencies $f = 0$ mm^{-1} and $f = 0.24$ mm^{-1}. For higher spatial frequencies, the relative error in SFD reflectance at the projection boundaries increases slightly, in spite of their higher sensitivity to short-range photons.

3.2 Binning Error

Spatial resolution in diffuse optics is fundamentally limited by the underlying scattering and absorption properties and is clearly outperformed by the resolution of commercial CCD cameras. Therefore, binning of captured SFD images can achieve a reduction in pixel noise at the expense of unsubstantial pixel resolution. At the same time, binning is of additional benefit due to an increase in evaluation speed.

Apart from the reduction in spatial resolution, strong binning of SFD images before the computation of the AC value using Eq. (1) gives rise to errors in SFD reflectance. Similar to the Nyquist sampling criterion for signal transmission, spatial resolution of SFDI data should be large enough to guarantee several sampling points within one spatial oscillation. Otherwise, oscillations in SFD data are averaged out in the binning process. Due to its infinite spatial wavelength, the DC component ($f = 0$ mm^{-1}) is not affected by this error.

The relative error $\delta R_{\mathrm{Binning}}$ of SFD reflectance based on excessive binning scales inversely with the number of sampling points per spatial oscillation. In order to quantify the binning related error, three phase shifted sine waves were computationally binned with a particular bin size and the AC component was subsequently computed using Eq. (1). Repetition of this calculation for different bin sizes and oscillation frequencies gives

the error in the AC component dependent on the oscillation frequency and bin size. Equation (2) is a power law which was fitted to the computational results and which describes the binning related error to a high precision. It gives an estimate of the percentage error in AC reflectance based on the binning x (number of pixels per bin):

$$\delta R_{\text{Binning}} = 209 \left(\frac{flx}{N} \right)^{2.113}, \tag{2}$$

where N is the number of pixels in one-dimension and l is the corresponding projection length in millimeters.

As an example, a typical SFD camera image with resolution $N/l = 1024/(50 \text{ mm})$ along the direction of spatial oscillations with $f = 0.24 \text{ mm}^{-1}$ allows for binning of $x = 8$ pixels in order for the error in SFD reflectance to be below 1.4%. Note that excessive binning always underestimates the real SFD reflectance values. If only one AC component is used, the binning related error corresponds to an error in spatial frequency (see discussion in Sec. 3.4). In this case, the obtained relative errors in μ_a and μ'_s are both linearly proportional to the error in AC reflectance.

It is worth pointing out that for particularly high spatial frequencies, diffraction and aberration in the optical imaging system may be additional limiting factors for precise determination of the SFD reflectance signal.

3.3 Height Adjustment Error

Precise sample and camera positioning are a prerequisite for accurate measurement of SFD reflectance. Although sample movements also affect the projection geometry and may cause spatial frequency errors (see Sec. 3.4), we now focus on the effect of incorrect adjustment of the distance between sample and camera. Thereby, we assume that this error in camera height is static and equally large for the measurement of all spatial frequencies (i.e., $f = 0 \text{ mm}^{-1}$ and $f = 0.24 \text{ mm}^{-1}$) and phase projections.

Variations in height alter the camera aperture angle and thus the captured light intensity. The additional effect of defocusing of the camera image and also the variation of the detection acceptance angle for points with different lateral separation from the optical axis is neglected in the following analysis. For simplicity, we approximate the angle resolved reflectance by Lambert's law[23] and thus the intensity of SFD reflectance captured for a particular camera height h and aperture radius r is

$$\int_0^{2\pi} \int_0^{\alpha} \cos(\theta) \sin(\theta) \mathrm{d}\theta \mathrm{d}\varphi = \pi(1 - \cos^2(\alpha)), \tag{3}$$

with $\alpha = \arcsin(r/h)$. If the camera height is changed by a distance x, the relative change in reflectance δR_{Height} is equally large for all spatial frequencies. This relative change can be approximated using a Taylor expansion and is given in percent by the following expression:

$$\delta R_{\text{Height}} = -\frac{200r}{h^2} \frac{\cos(r/h)}{\sqrt{1 - \cos^2(r/h)}} x. \tag{4}$$

Note that Eq. (4) is unit-of-length independent. As an example, for a camera aperture radius of $r = 1.5$ cm and a camera
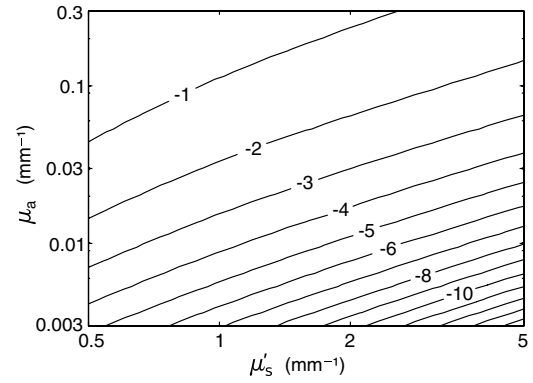

Fig. 9 Contour plot for the relative error in μ_a in percent based on a sample distance error which causes an increase in reflectance of 1%. According to Eq. (4), this error could be due to an unwanted decrease in sample-camera separation of $x = -1$ mm (assuming $h = 20$ cm and $r = 1.5$ cm).

height of $h = 20$ cm, a relative error in reflectance of 1% is obtained for height inaccuracy $x = -1$ mm. With respect to this sample calculation, we now present the impact on μ_a and μ'_s for a 1% increase in SFD reflectance. In Figs. 9 and 10, the relative errors in μ_a and μ'_s are given, respectively.

Generally, an increase in the SFD signal leads to an underestimation of absorption and an apparent increase in scattering. From Fig. 9, we learn that the error in μ_a is heavily dependent on the absorption and scattering regime and much larger than that of μ'_s in Fig. 10. Errors in both μ_a and μ'_s are almost proportional to the error in SFD reflectance as calculated by Eq. (4). Therefore, Figs. 9 and 10, which correspond to an error in reflectance of 1% can be used to approximate the error in μ_a and μ'_s based on any height inaccuracy. In this case, the contour values are scaled by the expected error in reflectance according to Eq. (4).

3.4 Spatial Frequency Error

Correct determination of the dimension of projected spatial frequencies is a prerequisite for accurate evaluation of SFD data. If only one AC frequency component together with the reflectance at $f = 0 \text{ mm}^{-1}$ (DC) is used to determine the absorption and scattering, potential errors in spatial frequency are linearly proportional to the obtained relative errors in μ_a
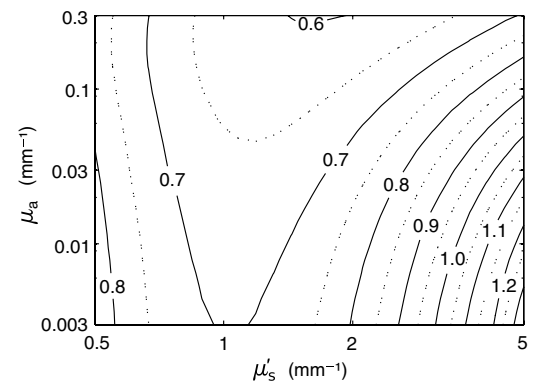

Fig. 10 Relative error in μ'_s in percent based on an incorrect separation of camera and sample. Similar to Fig. 9, the contour lines correspond to an increase in reflectance of 1% due to a reduction in the sample-camera distance.

and μ_s'. This is because scaling of μ_a and μ_s' by the same factor does not change the probability for photons to exit the media, but only scales the distance of their reflectance. Consequently, the obtained errors are independent of the absorption and scattering regime. This behavior is expressed by the following scaling property for SFD reflectance R_{SFD}

$$R_{SFD}(f, \mu_a, \mu_s) = R_{SFD}(cf, c\mu_a, c\mu_s), \qquad (5)$$

where c can be any positive real number.

Accordingly, a 5% inaccuracy in the projected spatial frequency pattern gives rise to 5% error in both μ_a and μ_s'. This underlines the necessity for accurate calibration of spatial frequencies. However, errors in spatial frequency do not only stem from improper calibration, but also from variations in the projection geometry. Furthermore, especially for oblique projection geometries, careful correction of frequency distortion is necessary.

4 Conclusion

Based on our systematic analysis on various sources of error in SFDI, we have provided the experimentalist with a realistic estimate of the significance of distinct experimental and theoretical parameters on derived scattering and absorption values. In contrast to our discrete analysis of single errors, realistic experiments will, however, always face an unknown combination of multiple errors. Prediction of the accuracy for any combination of errors is challenging, especially as many of the presented sources of errors are interdependent. For example, an incorrect height adjustment of the sample can also be the cause of spatial frequency errors and the error associated with the diffusion approximation is dependent on the actual scattering phase function of the sample. Generally, a potential compensation of errors in μ_a or μ_s' due to multiple sources of error should not mislead over the actual precision in both optical parameters. Due to their interdependence, uncertainties in μ_a and μ_s' for different sources of error do not add up like statistically independent variables. Instead, a more realistic error estimate is given by the sum of their absolute values. This is especially true, as more errors beyond the presented selection can arise.

Additional effects like camera nonlinearity, instability of the light source, the impact of surface roughness and specular reflections or more difficult experimental geometries, such as oblique projection or the use of multilayered media, can cause additional uncertainty. So far, little is known about the surface properties of biological tissue. Therefore, this and all related errors for diffuse optical imaging will be the focus of future work.

It is very common to employ calibration measurements with phantoms as an absolute reference for quantification in SFDI.[1,4,5,12,22] This approach properly accounts for the light projection intensity and the camera sensitivity. Unfortunately, most of the presented errors cannot be reliably reduced by the use of calibration measurements, unless reference phantom and final probe are equally affected by the existing errors. Even if the effect of various sources of errors is known, their dependence on the absorption and scattering regime and their interdependence render correction difficult. In some cases, calibration measurements on phantoms can even increase the overall uncertainty if phantom properties do not match that of subsequent specimens.

In conclusion, careful consideration should be made for the presented theoretical and experimental parameters in order to achieve the best accuracy in the obtained experimental results. Little importance is usually attached to parameters like the scattering asymmetry or the scattering phase function, even though they can cause significant quantitative and qualitative deviations in both μ_a and μ_s'. Our error analysis provides a means to estimate this uncertainty in μ_a and μ_s' based on the existence of various sources of errors.

References

1. A. Bassi et al., "Detection of inhomogeneities in diffusive media using spatially modulated light," *Opt. Lett.* **34**(14), 2156–2158 (2009).
2. D. J. Cuccia et al., "Modulated imaging: quantitative analysis and tomography of turbid media in the spatial-frequency domain," *Opt. Lett.* **30**(11), 1354–1356 (2005).
3. S. D. Konecky et al., "Quantitative optical tomography of sub-surface heterogeneities using spatially modulated structured light," *Opt. Exp.* **17**(17), 14780–14790 (2009).
4. J. R. Weber et al., "Noncontact imaging of absorption and scattering in layered tissue using spatially modulated structured light," *J. Appl. Phys.* **105**, 102028 (2009).
5. D. J. Cuccia et al., "Quantitation and mapping of tissue optical properties using modulated imaging," *J. Biomed. Opt.* **14**(2), 024012 (2009).
6. R. B. Saager, D. J. Cuccia, and A. J. Durkin, "Determination of optical properties of turbid media spanning visible and near-infrared regimes via spatially modulated quantitative spectroscopy," *J. Biomed. Opt.* **15**(1), 017012 (2010).
7. A. J. Lin et al., "Spatial frequency domain imaging of intrinsic optical property contrast in a mouse model of Alzheimer's disease," *Ann. Biomed. Eng.* **39**(4), 1349–1357 (2011).
8. D. Yudovsky and A. J. Durkin, "Spatial frequency domain spectroscopy of two layer media," *J. Biomed. Opt.* **16**(10), 107005 (2011).
9. A. M. Laughney et al., "System analysis of spatial frequency domain imaging for quantitative mapping of surgically resected breast tissues," *J. Biomed. Opt.* **18**(3), 036012 (2013).
10. S. L. Jacques, "Optical properties of biological tissues: a review," *Phys. Med. Biol.* **58**, R37–R61 (2013).
11. W. F. Cheong, S. A. Prahl, and A. J. Welch, "A review of the optical properties of biological tissues," *IEEE J. Quantum Electron.* **26**(12), 2166–2185 (1990).
12. A. Bassi et al., "Spatial shift of spatially modulated light projected on turbid media," *J. Opt. Soc. Am. A* **25**(11), 2833–2839 (2008).
13. A. Liemert and A. Kienle, "Spatially modulated light source obliquely incident on a semi-infinite scattering medium," *Opt. Lett.* **37**(19), 4158–4160 (2012).
14. A. Liemert and A. Kienle, "Exact and efficient solution of the radiative transport equation for the semi-infinite medium," *Sci. Rep.* **3**, 1–7 (2013).
15. L. G. Henyey and J. L. Greenstein, "Diffuse radiation in the Galaxy," *Astrophys. J.* **93**, 70–83 (1941).
16. L. O. Reynolds and N. J. McCormick, "Approximate two-parameter phase function for light scattering," *J. Opt. Soc. Am.* **70**(10), 1206–1212 (1980).
17. E. Berrocal et al., "Single scattering detection in turbid media using single-phase structured illumination filtering," *J. Eur. Opt. Soc. Rapid Publ.* **7**, 12015 (2012).
18. E. Alerstam, T. Svensson, and S. Andersson-Engels, "Parallel computing with graphics processing units for high-speed Monte Carlo simulation of photon migration," *J. Biomed. Opt.* **13**(6), 060504 (2008).
19. G. J. Tearney et al., "Determination of the refractive index of highly scattering human tissue by optical coherence tomography," *Opt. Lett.* **20**(21), 2258–2260 (1995).

20. H. Ding et al., "Refractive indices of human skin tissues at eight wavelengths and estimated dispersion relations between 300 and 1600 nm," *Phys. Med. Biol.* **51**, 1479–1489 (2006).
21. J.-C. Lai et al., "Complex refractive index measurement of biological tissues by attenuated total reflection ellipsometry," *Appl. Opt.* **49**(16), 3235–3238 (2010).
22. S. Gioux et al., "Three-dimensional surface profile intensity correction for spatially modulated imaging," *J. Biomed. Opt.* **14**(3), 034045 (2009).
23. A. Kienle and F. Foschum, "250 years Lambert surface: does it really exist?," *Opt. Exp.* **19**(5), 3881–3889 (2011).

Nico Bodenschatz is currently a PhD student in the Materials Optics and Imaging Group under supervision of Alwin Kienle at the University of Ulm. In 2012, he gained a master's degree in physics from Ulm University with thesis work at the Institute for Solid State Physics. In 2010, he completed his bachelor's degree in physics from the University of Konstanz with thesis work in soft matter physics at the University of Pennsylvania.

Arnd Brandes completed his bachelor's degree in information technology (BEng) in 2009 and his master's degree in biomedical engineering (MEng) in 2010. Since then he has been working as a PhD student in the Material Optics and Imaging Group under supervision of Alwin Kienle.

André Liemert received the diploma in mechatronics from the University of Applied Sciences, Ulm, in 2007. In 2011, he received the Dr.-Ing. degree in electrical engineering from the University of Ulm. From 2011 until present, he is working as a postdoctoral researcher in the Material Optics and Imaging Group of Alwin Kienle.

Alwin Kienle (PhD) is vice director (science) of the Institut für Lasertechnologien in der Medizin and Metechnik (ILM), Ulm, Germany, and head of the Materials Optics and Imaging Group at ILM. In addition, he is a professor at the University of Ulm. He studied physics and received his doctoral and habilitation degrees from University of Ulm. As postdoc, he worked with research groups in Hamilton, Canada, and in Lausanne, Switzerland.